SCIENTIFIC REPORTS

OPEN

Received: 28 July 2016
Accepted: 07 October 2016
Published: 24 October 2016

Enhanced methane steam reforming activity and electrochemical performance of $Ni_{0.9}Fe_{0.1}$-supported solid oxide fuel cells with infiltrated Ni-TiO_2 particles

Kai Li[1], Lichao Jia[2], Xin Wang[2], Jian Pu[2], Bo Chi[2] & Jian Li[2]

$Ni_{0.9}Fe_{0.1}$ alloy-supported solid oxide fuel cells with $NiTiO_3$ (NTO) infiltrated into the cell support from 0 to 4 wt.% are prepared and investigated for CH_4 steam reforming activity and electrochemical performance. The infiltrated $NiTiO_3$ is reduced to TiO_2-supported Ni particles in H_2 at 650 °C. The reforming activity of the $Ni_{0.9}Fe_{0.1}$-support is increased by the presence of the TiO_2-supported Ni particles; 3 wt.% is the optimal value of the added NTO, corresponding to the highest reforming activity, resistance to carbon deposition and electrochemical performance of the cell. Fueled wet CH_4 at 100 mL min^{-1}, the cell with 3 wt.% of NTO demonstrates a peak power density of 1.20 W cm^{-2} and a high limiting current density of 2.83 A cm^{-2} at 650 °C. It performs steadily for 96 h at 0.4 A cm^{-2} without the presence of deposited carbon in the $Ni_{0.9}Fe_{0.1}$-support and functional anode. Five polarization processes are identified by deconvoluting and data-fitting the electrochemical impedance spectra of the cells under the testing conditions; and the addition of TiO_2-supported Ni particles into the $Ni_{0.9}Fe_{0.1}$-support reduces the polarization resistance of the processes ascribed to CH_4 steam reforming and gas diffusion in the $Ni_{0.9}Fe_{0.1}$-support and functional anode.

On-cell methane (CH_4) reforming in Ni-based anodes is an attractive option for directly using CH_4-based fuels for solid oxide fuel cells (SOFCs) with high fuel efficiency and simplified system design[1,2]. CH_4 steam reforming is a catalytic process for commercial production of H_2 or syngas at a H_2:CO molar ratio of 3:1 according to the endothermic reaction of

$$CH_4 + H_2O \rightarrow CO + 3H_2 \ \Delta H^0 = 206.1\,kJ/mol \quad (1)$$

Excessive addition of H_2O will further converts CO to CO_2 by the slightly exothermic water gas shift (WGS) reaction[3–5].

$$CO + H_2O \rightarrow CO_2 + H_2 \ \Delta H^0 = -41.2\,kJ/mol \quad (2)$$

If these reactions are taking place in the anode of an SOFC, H_2 is consumed via electrochemical oxidation to generate electrical power[6,7], forming by-product of H_2O. Such *in-situ* formed H_2O is simultaneously used for CH_4 steam reforming, which reduces the amount of externally added H_2O to improve the electrical efficiency of the SOFC system.

[1]School of Materials Science and Engineering, Xi'an Shiyou University, Xi'an 710065, China. [2]Center for Fuel Cell Innovation, State Key Laboratory for Materials Processing and Die & Mould Technology, School of Materials Science and Engineering, Huazhong University of Science and Technology, Wuhan 430074, China. Correspondence and requests for materials should be addressed to B.C. (email: chibo@hust.edu.cn)

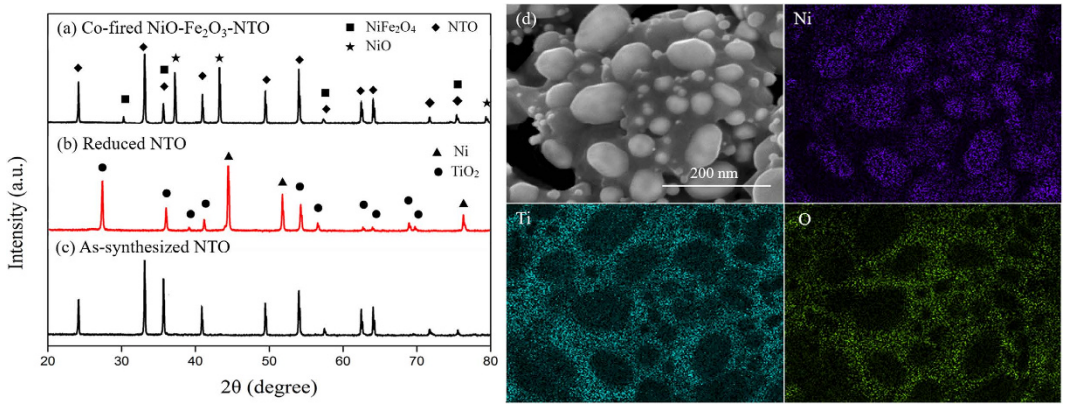

Figure 1. XRD patterns of (**a**) as-synthesized NTO powder (1000 °C for 2 h in air), (**b**) reduced NTO powder (650 °C for 2 h in H_2), (**c**) co-fired NiO-Fe_2O_3-NTO powder mixture (1000 °C for 2 h in air) and (**d**) EDS mappings of Ni, Ti and O for TiO_2-supported Ni particles.

However, for on-cell CH_4 reforming in Ni-based anodes, coking is frequently observed in the anode when steam/carbon (H_2O/CH_4) ratio is low, since Ni catalyzes CH_4 decomposition that produces deposited carbon in the form of filament or particle via either CH_4 cracking or the Boudouard reactions as follow

$$CH_4 \rightarrow C + 2H_2 (CH_4 \text{cracking}) \quad (3)$$

$$2CO \rightarrow CO_2 + C (\text{Boudouard reaction}) \quad (4)$$

The soot-like carbon particles are distributed on the surface of Ni particles, occupying the active sites for electrochemical reaction and the pores for fuel gas transport[8]; and the carbon filaments formed by carbon diffusion into/precipitation out the Ni particles[9] disintegrate the Ni-cermet anode by lifting out the Ni particles from the anode (dusting).

It has been demonstrated that infiltration of oxides, such as rare-earth doped CeO_2[10–12], BaO[13] and CaO-MgO[14], into the Ni-based anode is an effective way to enhance its coking resistance by suppressing carbon formation and promoting steam-carbon reactions. Although TiO_2 has not been investigated in SOFCs, it was used as a support in catalysts for steam reforming of hydrocarbons (methanol[15], ethanol[16] and glycerol[17]), CO_2 reforming of CH_4[15,18] and CO oxidation[19]; and high coking resistance was demonstrated in CH_4[20] and ethanol[16] reforming. Stimulated by these investigations, TiO_2 was evaluated in direct-CH_4 SOFCs for the enhancement of CH_4 on-cell reforming in the present study.

Compared with electrolyte- and electrode-supported SOFCs, metal-supported SOFCs have some advantages in the aspects of electrical/thermal conductivity and mechanical ductility; consequently, the temperature distribution in and tolerance to thermal cycle of the cell are improved[21,22]. In our previous study, Ni-Fe alloy-supported SOFCs were investigated with the purpose of using wet (3 vol.% H_2O) CH_4 as the fuel, and high performance (0.6 V at 0.4 A cm^{-2} and 650 °C for 50 h[7]) was achieved. However, the $Ni_{0.9}Fe_{0.1}$-support used was not fully resistant to carbon deposition, and carbon lumps were formed in its large pores. In order to develop metal-supported direct-hydrocarbon SOFCs, $Ni_{0.9}Fe_{0.1}$-supported SOFCs were prepared with $NiTiO_3$ infiltrated into the $Ni_{0.9}Fe_{0.1}$-support. It was expected that $NiTiO_3$ would be reduced into TiO_2-supported Ni particles in H_2 to enhance CH_4 reforming activity and resistance to carbon deposition of the $Ni_{0.9}Fe_{0.1}$-supported cells.

Results

Materials and cell characterization. Figure 1a–c show the XRD patterns of the as-synthesized and reduced NTO and co-fired powder mixture of NiO, Fe_2O_3 and NTO. The as-synthesized NTO demonstrated a perovskite structure of $NiTiO_3$ (JCPDF# 76-0334), and the reduced product was a mixture of TiO_2 (JCPDF# 21-1276) and Ni (JCPDF# 04-0850). Figure 1d shows EDS mappings of Ni, Ti and O for the mixture. It indicates that the bright granules in surface are identified by EDS as metallic Ni, and the dark areas rich in Ti and O. Based on this result, it is expected that the infiltrated NTO particles on the surface of the scaffold of the cell support be reduced into TiO_2-supported Ni (0) particles. It was confirmed in our previous study[7] that the sintered NiO-Fe_2O_3 cell support is consisted of two phases of NiO and $NiFe_2O_4$, and its reduced form is $Ni_{0.9}Fe_{0.1}$ alloy. With NTO powder added, the co-fired NiO-Fe_2O_3-NTO mixture contained NiO, $NiFe_2O_4$ and NTO (Fig. 1a), which indicates that NTO was chemically compatible with NiO and $NiFe_2O_4$ at temperatures up to 1000 °C and would remain as an independent phase in the scaffold of the sintered NiO-$NiFe_2O_4$ cell support.

Shown in Fig. 2 is the SEM microstructure of the fractured cross-section of the reduced cell with $Ni_{0.9}Fe_{0.1}$-support. As observed previously[7], the sintered NiO-$NiFe_2O_4$ cell support was reduced into a porous scaffold (58%) with a bimodal pore distribution. The average size of the large pores was around 10 μm, which is beneficial for fuel gas transport in the support to the functional anode; and the small pores within the stem of the scaffold give a high specific surface area that is beneficial for CH_4 reforming reaction. The Ni-GDC functional anode was approximately 1αm thick and intimately in contact with the fully dense GDC electrolyte (~10 μm)

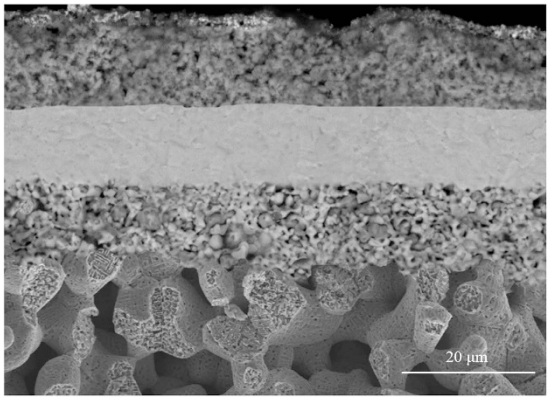

Figure 2. Fractured cross-sectional microstructure of a $Ni_{0.9}Fe_{0.1}$-support cell.

and the porous cell support (~1 mm). The thickness of the BSCF-LSM cathode was averagely 15 μm. Figure 3 respectively present the microstructure of the sintered and reduced cell supports with various amounts of infiltrated NTO from 1 to 4 wt.% of the weight of the half cell (NiO-Fe_2O_3 anode-support | NiO-GDC anode | GDC electrolyte).

Reforming activity of infiltrated $Ni_{0.9}Fe_{0.1}$-supports. CH_4 reforming in the $Ni_{0.9}Fe_{0.1}$-support is a chemical process that *in situ* produces H_2, which is electrochemically oxidized on the functional Ni-GDC anode to generate electrical power with byproduct of steam via the reaction of

$$H_2 + O^{2-} \rightarrow H_2O + 2e \quad (5)$$

Thus the reforming activity of the $Ni_{0.9}Fe_{0.1}$-support is of critical importance for the performance of the cell with on-cell CH_4 reforming. Figure 4 shows the CH_4 conversion rate and reforming product distribution at 650 °C in the $Ni_{0.9}Fe_{0.1}$-supports loaded with different amounts of TiO_2-supported Ni particles. The initial values of CH_4 conversion rate were approximately 50%, 55%, 58%, 61% and 60% for the $Ni_{0.9}Fe_{0.1}$-supports loaded with 0%, 1%, 2%, 3% and 4 wt.% of NTO (designated as 0NTO, 1NTO, 2NTO, 3NTO and 4NTO), respectively. This indicates that the addition of TiO_2-suported Ni particles in the $Ni_{0.9}Fe_{0.1}$-support promoted its reforming activity with a limit of 3 wt.% NTO, more than which the conversion rate decreased, possibly due to the over-cover of the reforming active sites on the surface of the $Ni_{0.9}Fe_{0.1}$ scaffold by TiO_2 and increased surface area of the small Ni particles for carbon deposition. The CH_4 conversion rate of 0NTO, 1NTO, 2NTO and 4NTO decreased obviously with time after approximately 12 h, only which of 3NTO remained relatively stable during the testing period of 24 h. The main reforming products were H_2, CO and CO_2 (Fig. 4b–d), and their concentrations varied accordingly with the testing time.

Cell performance. The cells with NTO-infiltrated $Ni_{0.9}Fe_{0.1}$-supports were evaluated at 650 °C with wet CH_4 (3 vol.% H_2O) as the fuel; Fig. 5 shows their initial I-V-P curves. The open circuit voltage (OCV) of all the cells was around 0.78 V, due to the partial electronic conduction of GDC electrolyte[23]. The maximum power densities increased from 0.99 to 1.20 W cm^{-2} as the NTO loading was increased from 0 to 3 wt.%. Further increasing NTO loading to 4 wt.%, it decreased to 1.17 W cm^{-2}. Figure 6 shows the initial impedance spectra of the cells under a current density of 0.4 A cm^{-2} (Fig. 6a), from which the ohmic (R_O) and polarization (R_P) resistances were determined, and the corresponding distributions of relaxation time (DRT, Fig. 6b)[24,25]. The value of R_O of each cell was similar, around 0.063 Ω cm^{-2}, and that of R_P varied in an opposite direction to the cell voltage and power density. This tendency of cell performance change with the amount of loaded NTO in the $Ni_{0.9}Fe_{0.1}$-support is consistent with that of the activity for CH_4 steam reforming shown above, which suggests that cell performance improvement is due to the increased reforming activity of the $Ni_{0.9}Fe_{0.1}$-support and the consequent increase in the amount of H_2 available for the anode reaction.

The DRT $G(\tau)$ was associated with the impedance Z(w) by the following expression:

$$Z(w) = Z'(\infty) + \int_0^\infty \frac{G(\tau)}{1 + jw\tau} d\tau \quad (6)$$

Where $G(\tau)$ is defined as the DRT of impedance Z, τ is relaxation time, $Z'(\infty)$ is the limitation of the real part of Z as angular frequency w approaches infinity. Consequently, impedance could be represented as series connection of infinite number of parallel polarization resistor $G(\tau)d\tau$ and a capacitor $\tau/G(\tau)d\tau$. For a more detailed description of DRT method and application were referred[26].

After the initial evaluation, all the cells were further tested at 650 °C and a constant current density of 0.4 A cm^{-2} for up to 96 h; the results are shown in Fig. 7. The improvement on cell performance durability is in consistence with that on CH_4 steam reforming activity. The cells with 0NTO, 1NTO, 2NTO and 4NTO $Ni_{0.9}Fe_{0.1}$-supports performed 67, 78, 90 and 96 h before the sudden drop of the cell voltage; and the cell with 3NTO $Ni_{0.9}Fe_{0.1}$-support outperformed the others, degrading linearly at a slow rate of 0.5 mV h^{-1} during the testing period. Post-test examination confirmed that the sudden voltage drop at the end of the test was caused by cell

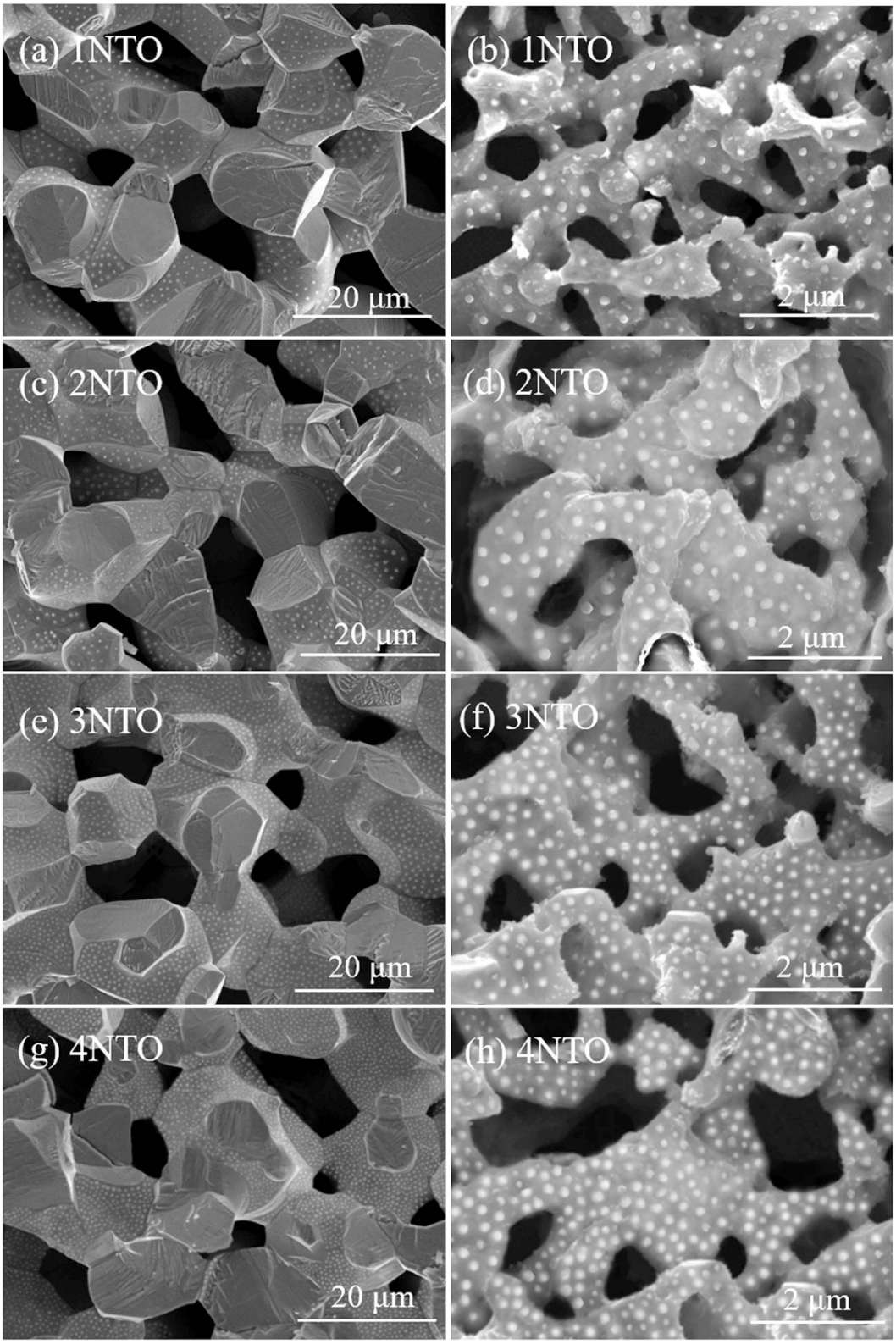

Figure 3. Fractured cross-sectional microstructure of (**a**) sintered and (**b**) reduced $Ni_{0.9}Fe_{0.1}$-supports with various amounts of infiltrated NTO.

disintegration due to dusting of the $Ni_{0.9}Fe_{0.1}$-support. The linear voltage decrease, at nearly the same rate for all the cells, may represent the intrinsic cell degradation that needs further understanding for mechanism, whereas the non-linear voltage decrease is attributed to carbon deposition in the $Ni_{0.9}Fe_{0.1}$-support and functional anode.

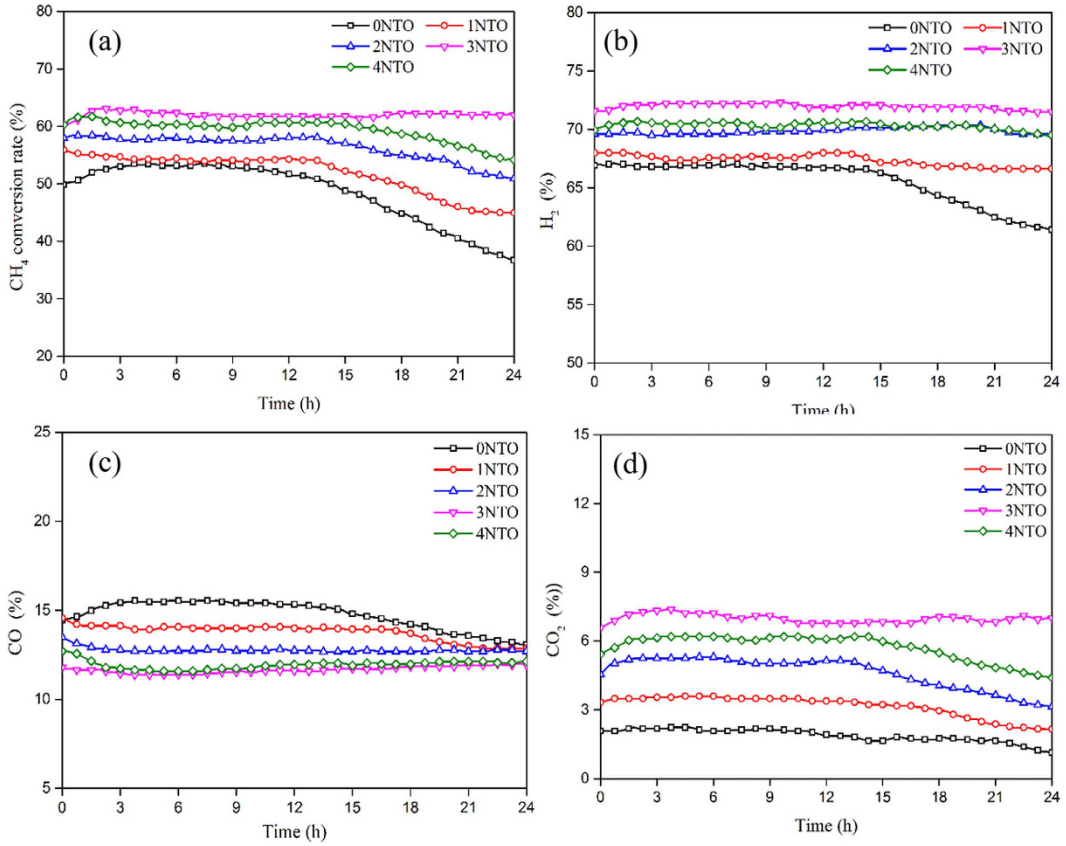

Figure 4. CH_4 steam reforming of $Ni_{0.9}Fe_{0.1}$-supports with various amounts of infiltrated NTO at 650 °C and 1:1 CH_4 to H_2O ratio: (**a**) CH_4 conversion rate and (**b**) H_2, (**c**) CO and (**d**) CO_2 concentrations in reformate.

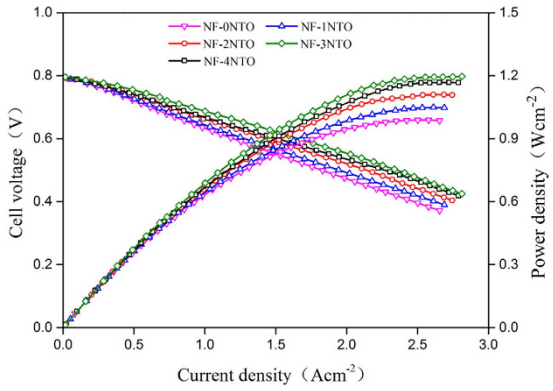

Figure 5. I-V-P curves of $Ni_{0.9}Fe_{0.1}$-supported cells with various amounts of infiltrated NTO in the $Ni_{0.9}Fe_{0.1}$-supports at 650 °C with wet CH_4 as the fuel.

Since the deposited carbon remained in the cell, its amount can be quantified from the temperature-programmed oxidation (TPO) profile of the post-test cells, as shown in Fig. 8. The area of CO_2 peak, an indication of the amount of CO_2 formed from deposited carbon, were 7.89×10^{-8}, 6.93×10^{-8}, 2.61×10^{-8} and 3.15×10^{-8} for the cells with 1NTO, 2NTO, 3NTO and 4NTO $Ni_{0.9}Fe_{0.1}$-supports, respectively. These values support the explanation of the durability testing results and indicate that the cell with 3NTO anode-support is the most resistant to carbon deposition among the cells investigated.

Discussion

According to previous studies[19,27], the effectiveness of TiO_2 on improving reforming activity can be attributed to its enhanced capability of H_2O adsorption and consequently the coking resistance. It is the H_2O adsorbed on the catalyst that increases the reforming activity[19]; and the prevalent presence of subsurface defects of TiO_2 in reduced atmosphere, such as oxygen vacancies and Ti interstitials, enhances H_2O adsorption due to surface relaxation and

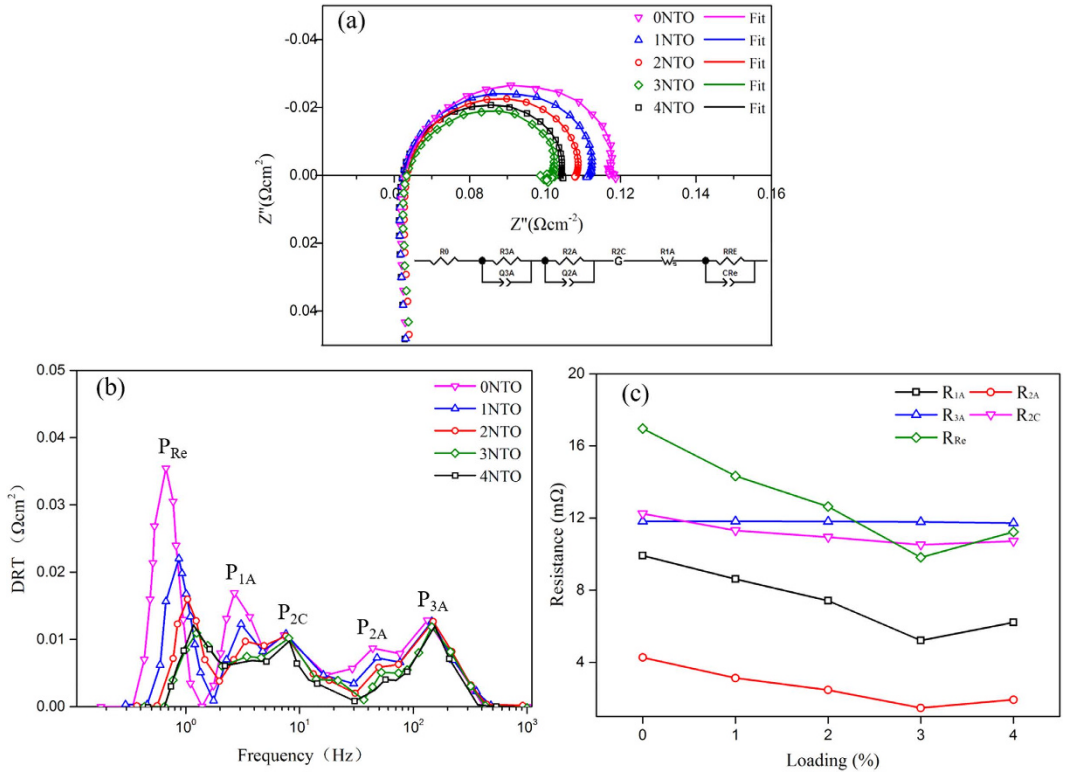

Figure 6. Impedance spectra at 650 °C and 0.4 A cm^{-2} (**a**), corresponding DRT (**b**) and polarization resistance of deconvoluted processes (**c**) of the $Ni_{0.9}Fe_{0.1}$-supported cells with various amounts of NTO in the $Ni_{0.9}Fe_{0.1}$-supports.

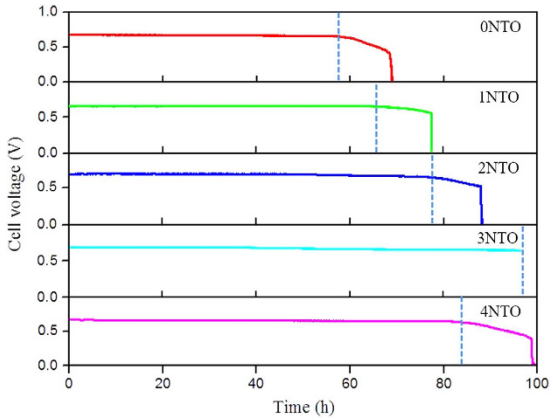

Figure 7. Cell voltage of wet CH_4 fueled $Ni_{0.9}Fe_{0.1}$-supported cells with various amounts of NTO in the $Ni_{0.9}Fe_{0.1}$-supports as a function of testing time at 650 °C and a constant current density of 0.4 Acm^{-2}.

charge localization. On-cell methane reforming, constant adsorption of H_2O in anode will shift the equilibrium reaction of Eqs (1) and (2) in a forward direction. Therefore, H_2 and CO_2 concentration increases whereas CO concentration decrease with increase in the amount of H_2O. The increase in H_2 concentration and the decrease in CO concentration subsequently prevent possible carbon formation by shifting Boudard reaction (Eq. 3) and decomposition of CH_4 (Eq. 4) in a backward direction. In addition, the excess H_2 reacts with oxygen ion from electrolyte to product electrical power and steam, which enhances the water-gas shift reaction and retards CH_4 decomposition. In additional to the contribution of H_2O adsorption on TiO_2, the TiO_2-supported Ni particles on the surface of $Ni_{0.9}Fe_{0.1}$ scaffold are also considered to increase the reforming activity, due to its known tendency to form a strong metal-support interaction (SMSI) between TiO_2 support and Ni metal and widely used catalyst of CH_4 and ethanol steam reforming[16,28].

Based on the DRT shown in Fig. 6b and the results reported in a previous investigation[25], five polarization processes were identified for individual cells, which are two high-frequency processes ascribed to the gas diffusion

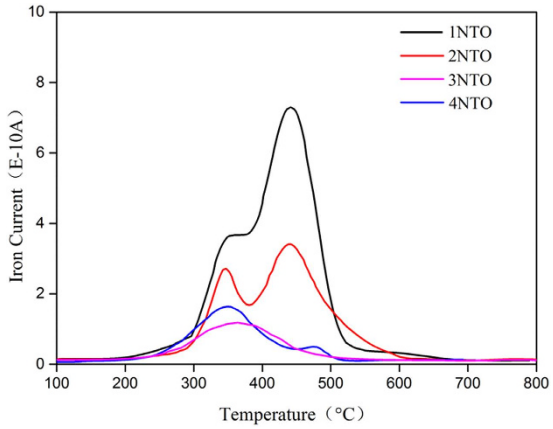

Figure 8. O_2-TPO profiles of NTO infiltrated cells tested with wet CH_4 as the fuel at 650 °C for up to 96 h.

and charge transfer/ionic transport within the functional anode (P_{2A} and P_{3A}), one high-frequency process associated with oxygen surface exchange and bulk diffusion within the BSCF-LSM cathode (P_{2C}), one low-frequency process related to mass transport in the $Ni_{0.9}Fe_{0.1}$-support (P_{1A}) and one low-frequency process attributed to CH_4 reforming in the $Ni_{0.9}Fe_{0.1}$-support (P_{Ref}). The contribution of each process to the total polarization resistance was obtained by data fitting the impedance spectra (Fig. 6a) using the complex nonlinear least-squares method and an equivalent circuit (inset in Fig. 6a) consisting of an ohmic resistor R_O, two RQ elements for P_{2A} and P_{3A}, a Gerischer element (G) for P_{2C}, a generalized finite length Warburg element (W) for P_{1A} and another RQ element for P_R. The change of the polarization resistance for each process, R_{1A}, R_{2A}, R_{3A}, R_{2C} and R_{Ref}, with the amount of loaded NTO is demonstrated in Fig. 6c. R_{3A} and R_{2C} remained almost unaffected by NTO infiltration, since the cathode was identical for all the cells, and the electrochemical reaction in the functional Ni-GDC anodes was the same reaction of H_2 oxidation[25] regardless of the amount of NTO loaded in the $Ni_{0.9}Fe_{0.1}$-support. The resistance of diffusion of reformate in the $Ni_{0.9}Fe_{0.1}$-support and Ni-GDC functional anode, R_{1A} and R_{2A}, decreased with increasing NTO amount till 3 wt.% and then increased at 4 wt.%, which reflects the amount change of H_2 in the reformate. It is expected that higher concentration of H_2 in the reformate lead to lower diffusion resistance in porous cell support and functional anode due to the high diffusivity of H_2. R_{Ref} is assigned to CH_4 steam reforming process; its change with the amount of loaded NTO in the $Ni_{0.9}Fe_{0.1}$-support is consistent with that of the reforming activity. According to the data-fitting results and discussions, it may be concluded that the cell performance improvement with NTO infiltration in the $Ni_{0.9}Fe_{0.1}$-support is attributed to the improved CH_4 reforming activity and the decreased potential of carbon deposition; consequently the polarization resistances related to CH_4 reforming and reformate transport processes are decreased.

NTO infiltration into $Ni_{0.9}Fe_{0.1}$-supports was investigated with the purpose of enhancing CH_4 steam reforming activity, carbon deposition resistance and cell performance. Based on the obtained results and discussion, the following conclusions are drawn.

(1) The activity of the $Ni_{0.9}Fe_{0.1}$-support for CH_4 steam reforming is enhanced by infiltrated NTO, which is reduced into TiO_2-supported Ni (0) particles in H_2. The TiO_2 improves the resistance to carbon deposition by adsorbing H_2O, while the supported small Ni particles promote CH_4 decomposition.
(2) 3 wt.% of the weight of the half cell (anode-support | functional anode | electrolyte) is the optimal value for the amount of NTO infiltrated into the $Ni_{0.9}Fe_{0.1}$-support. Increased CH_4 reforming activity lead to the improvement of cell performance, durability and resistance to carbon deposition.
(3) The overall cell polarization resistance is contributed by five polarization processes associated with CH_4 reforming (P_{ref}), mass transport in anode-support (P_{1A}), gas diffusion in functional anode (P_{2A}), charge transfer within functional anode (P_{3A}), and oxygen surface exchange and bulk diffusion within cathode (P_{2C}). The addition of NTO into the $Ni_{0.9}Fe_{0.1}$-support reduces the polarization resistance of P_{ref}, P_{1A} and P_{2A}.

Methods

Cell fabrication. $Ni_{0.9}Fe_{0.1}$-supported cells were fabricated by tape casting-screen printing-sintering process. NiO (Haite Advanced Materials) and Fe_2O_3 (Sinopharm) powders were mixed at a Ni:Fe molar ratio of 9:1 and ball-milled for 24 h in xylene/ethanol solvent with fish oil (Richard E. Mistler, Inc.) as the dispersant, corn starch as the pore former, poly vinyl butyral (Solutia Inc.) as the binder and butyl benzyl phthalate and poly alkylene glycol (Solutia Inc.) as the plasticizer. The prepared slurry was cast into a tape with a dry thickness of ~1.2 mm, which was then die-cut into discs (25 mm in diameter) as the cell support, on which NiO (Inco)-GDC (10 mol.% Gd-doped CeO_2, NIMTE, CAS) functional anode and GDC electrolyte were screen printed in sequence, followed by sintering at 1450 °C in air for 5 h. $La_{0.8}Sr_{0.2}MnO_3$-coated $Ba_{0.5}Sr_{0.5}Co_{0.8}Fe_{0.2}O_3$ (LSM-BSCF) cathode[29] was then screen-printed on the sintered GDC electrolyte and sintered in air at 1050 °C for 2 h.

To introduce TiO_2-supported Ni particles onto the stem of NiO-Fe_2O_3 scaffold (~40% porosity[30]), an aqueous solution containing Ti and Ni ions at the stoichiometric concentration of $NiTiO_3$ (NTO) was prepared as follow. Tetrabutyl titanate ($C_{16}H_{36}O_4Ti$, Sinopharm) was dissolved in a dilute nitric acid aqueous solution under

stirring, and then stoichiometric amount of Ni nitrate ($Ni(NO_3)_2{\cdot}6H_2O$, Sinopharm) was added prior to the addition of citric acid (CA) and ethylenediamine tetraacetic acid (EDTA) as the chelants. The molar ratio of metal ions:CA:EDTA in the solution was 1:1:1.5. Ammonia solution was used to adjust the pH value of the solution to approximately 7. Such prepared solution was infiltrated into the pores of the sintered NiO-Fe_2O_3 scaffold and calcined in air at 1000 °C for 2 h to form crystallized NTO nano particles. This infiltration process was repeated to achieve the desired amounts of loaded NTO in the scaffold. The crystal structure of NTO and its chemical reactivity with NiO and Fe_2O_3 were determined by X-ray diffraction (XRD, X'Pert) using a NiO-Fe_2O_3-NTO powder mixture co-fired in air at 1000 °C for 2 h. The NTO powder was obtained by calcining the dried solution in air at 1000 °C for 2 h, and its reduced form (650 °C in H_2 for 2 h) was characterized by XRD for phase identification and examined by using a scanning electron microscope (SEM, FEI sirion 200).

Steam reforming activity evaluation. To evaluate the catalytic activity of the infiltrated $Ni_{0.9}Fe_{0.1}$-support for CH_4 steam reforming, the NiO-Fe_2O_3 support sintered at 1450 °C in air for 5 h was sealed in a ceramic housing using a Ceramabond^{TM} sealant (Aremco Product, Inc.) and reduced at 650 °C in H_2 for 2 h. Then a mixture of 10% CH_4, 10% H_2O and 80% He was fed into the porous support at a constant rate of 100 ml min^{-1}. The steam content in the mixture was controlled by flowing dry CH_4 and He gases through a saturator containing distilled water at 50 °C according to the following equation[31].

$$log\,(p_{H_2O}) = \frac{-2961}{T_{bubbler}} - 5.13\ \ log\,(T_{bubbler}) + 21.133 \tag{7}$$

Compositional analysis of the effluent gas from the reactor was conducted with an on-line Pfeiffer Vacuum Mass Spectrometer. The steam reforming was performed at temperatures between 500 and 700 °C, and the CH_4 conversion rate (X (%)) was estimated using the following equation.

$$\mathrm{x}(\%) = \frac{[CO] + [CO_2]}{[CO] + [CO_2] + [CH_4]} \tag{8}$$

Cell testing and characterization. The cell performance was evaluated at 650 °C with wet (3 mol.% H_2O) CH_4 as the fuel and ambient air as the oxidant at a flow rate of 100 ml min^{-1}. Using a power supply of Solartron 1480A in 4-probe mode, the current density (i)–voltage (V)-power density (P) polarization curves were obtained at a scanning rate of 5 mVs^{-1} from 0 to 1 V, and electrochemical impedance spectra (EIS) were acquired within a frequency range from 100 KHz to 0.01 Hz and an AC signal amplitude of 10 mV. The microstructure of the cell was examined by using a SEM. The resistance to carbon deposition of (the amount of deposited carbon in) the $Ni_{0.9}Fe_{0.1}$-supported cell was characterized by temperature-programmed-oxidation (TPO) method at a flow rate of 20 ml min^{-1} of pure oxygen.

References

1. Chen, Y. *et al.* Direct-methane solid oxide fuel cells with hierarchically porous Ni-based anode deposited with nanocatalyst layer. *Nano Energy*. **10,** 1–9 (2014).
2. Kan, H. & Lee, H. Enhanced stability of Ni–Fe/GDC solid oxide fuel cell anodes for dry methane fuel. *Catalysis Communications*, **12,** 36–39 (2010).
3. Angeli, S. D., Monteleone, G., Giaconia, A. & Lemonidou, A. A. State-of-the-art catalysts for CH_4 steam reforming at low temperature. *International Journal of Hydrogen Energy*, **39,** 1979–1997 (2014).
4. Angeli, S. D., Pilitsis, F. G. & Lemonidou, A. A. Methane steam reforming at low temperature: Effect of light alkanes' presence on coke formation. *Catalysis Today*, **242,** 119–128 (2015).
5. Rakass, S., Oudghiri, H. H., Rowntree, P. & Abatzoglou, N. Steam reforming of methane over unsupported nickel catalysts. *Journal of Power Sources*, **158,** 485–496 (2006).
6. Andersson, M., Paradis, H., Yuan, J. L. & Sunden, B. Review of catalyst materials and catalytic steam reforming reactions in SOFC anodes. *International Journal of Energy Research*. **35,** 1340–1350 (2011).
7. Li, K. *et al.* Methane on-cell reforming in nickel–iron alloy supported solid oxide fuel cells. *Journal of Power Sources*, **284,** 446–451 (2015).
8. Lu, M., Lv, P., Yuan, Z. & Li, H. The study of bimetallic Ni–Co/cordierite catalyst for cracking of tar from biomass pyrolysis. *Renewable Energy*. **60,** 522–528 (2013).
9. Yang, R. T. & Chen, J. P. Mechanism of carbon filament growth on metal catalysts *Journal of Catalysis*. **115,** 52–64 (1989).
10. Chen, Y. *et al.* $Sm_{0.2}(Ce_{1-x}Ti_x)_{0.8}O_{1.9}$ modified Ni–yttria-stabilized zirconia anode for direct methane fuel cell *Journal of Power Sources*. **196,** 4987–4991 (2011).
11. Wang, W., Jiang, S. P., TokA, I. Y. & Luo, L. GDC-impregnated Ni anodes for direct utilization of methane in solid oxide fuel cells. *Journal of Power Sources*. **159,** 68–72 (2006).
12. Ding, D., Liu, Z., Li, L. & Xia, C. An octane-fueled low temperature solid oxide fuel cell with Ru-free anodes. *Electrochemistry Communications*. **10,** 1295–1298 (2008).
13. La Rosa, D. *et al.* Mitigation of carbon deposits formation in intermediate temperature solid oxide fuel cells fed with dry methane by anode doping with barium. *Journal of Power Sources*. **193,** 160–164 (2009).
14. York, A. P. E., Xiao, T., Green, M. L. H. & Claridge, J. B. Methane Oxyforming for synthesis gas production. *Catalysis Reviews*. **49,** 511–560 (2007).
15. Yan, Q. G. *et al.* Activation of methane to syngas over a Ni/TiO_2 catalyst. *Applied Catalysis a-General*. **239,** 43–58 (2003).
16. Rossetti, I. *et al.* TiO_2-supported catalysts for the steam reforming of ethanol *Applied Catalysis a-General*. **477,** 42–53 (2014).
17. Adhikari, S., Fernando, S. D. & Haryanto, A. Hydrogen production from glycerin by steam reforming over nickel catalysts. *Renewable Energy*. **33,** 1097–1100 (2008).
18. Shinde, V. M. & Madras, G. Catalytic performance of highly dispersed Ni/TiO_2 for dry and steam reforming of methane. *Rsc Advances*. **4,** 4817–4826 (2014).
19. Daté, M. & Haruta, M. Moisture effect on CO oxidation over Au/TiO_2 catalyst. *Journal of Catalysts*. **201,** 221–224 (2001).
20. Bradford, M. C. J. & Vannice, M. A. CO_2 reforming of CH_4 over supported Pt catalysts. *Journal of Catalysts*. **173,** 157–171 (1998).
21. Tucker, M. C. Progress in metal-supported solid oxide fuel cells: A review. *Journal of Power Sources*. **195,** 4570–4582 (2010).

22. Matus, Y., Dejonghe, L., Jacobson, C. & Visco, S. Metal-supported solid oxide fuel cell membranes for rapid thermal cycling. *Solid State Ionics*. **176,** 443–449 (2005).
23. Park, H. C. & Virkar, A. V. Bimetallic (Ni–Fe) anode-supported solid oxide fuel cells with gadolinia-doped ceria electrolyte. *Journal of Power Sources*. **186,** 133–137 (2009).
24. Leonide, A., Sonn, V., Weber, A. & Ivers-Tiffée, E. Evaluation and modeling of the cell resistance in anode-supported solid oxide fuel cells. *Journal of the Electrochemical Society*. **155,** B36 (2008).
25. Kromp, A., Geisler, H., Weber, A. & Ivers-Tiffee, E. Electrochemical impedance modeling of gas transport and reforming kinetics in reformate fueled solid oxide fuel cell anodes. *Electrochimica Acta*. **106,** 418–424 (2013).
26. Zhang, Y. X., Chen, Y., Yan, M. F. & Chen, F. L. Reconstruction of relaxation time distribution from linear electrochemical impedance spectroscopy. *Journal of Power Sources*. **283,** 464–477 (2015).
27. Aschauer, U. *et al.* Influence of subsurface defects on the surface reactivity of TiO_2: water on anatase (101). *J. Phys. Chem. C*. **114,** 1278–1284 (2010).
28. Rui, Z., Feng, D., Chen, H. & Ji, H. Anodic TiO_2 nanotube array supported nickel–noble metal bimetallic catalysts for activation of CH_4 and CO_2 to syngas. *International Journal of Hydrogen Energy*. **39** 16252–16261 (2014).
29. Meng, L. *et al.* High performance $La_{0.8}Sr_{0.2}MnO_3$-coated $Ba_{0.5}Sr_{0.5}Co_{0.8}Fe_{0.2}O_3$ cathode prepared by a novel solid-solution method for intermediate temperature solid oxide fuel cells. *Chinese Journal of Catalysis*. **35,** 38–42 (2014).
30. Li, K. *et al. International Journal of Hydrogen Energy*, **39,** 19747–19752 (2014).
31. Hua, B. *et al.* Oxidation behavior and electrical property of a Ni-based alloy in SOFC anode environment. *Journal of the Electrochemical Society*. **156,** B1261 (2009).

Acknowledgements

This research was financially supported by Natural Science Foundation of China (51472099 and 51672095). The SEM and XRD characterizations were assisted by the Analytical and Testing Center of Huazhong University of Science and Technology.

Author Contributions

K.L., L.J. and X.W. conducted the experiments and prepared the manuscript; J.P. and J.L. provided suggestions to the experiments; B.C. initiated the study, discussed the results and revised the manuscript.

Additional Information

Competing financial interests: The authors declare no competing financial interests.

How to cite this article: Li, K. *et al.* Enhanced methane steam reforming activity and electrochemical performance of $Ni_{0.9}Fe_{0.1}$-supported solid oxide fuel cells with infiltrated Ni-TiO_2 particles. *Sci. Rep.* **6**, 35981; doi: 10.1038/srep35981 (2016).